ACS OMEGA

Open Access

http://pubs.acs.org/journal/acsodf

Article

Vetting of New 2,5-Bis (2,2,2-trifluoroethoxy) Phenyl-Linked 1,3-Thiazolidine-4-one Derivatives as AURKA and VEGFR-2 Inhibitor Antiglioma Agents Assisted with In Vitro and In Silico Studies

Sathyanarayana D Shankara, Arun M. Isloor,* Pavan K. Jayaswamy, Praveenkumar Shetty, Debashree Chakraborty, and Pushyaraga P. Venugopal

Cite This: *ACS Omega* 2023, 8, 43596−43609

Read Online

ACCESS | Metrics & More | Article Recommendations | Supporting Information

ABSTRACT: The bioactivity of 1,3-thiazolidin-4-one derivatives with a 2,5-bis (2,2,2-trifluoroethoxy) phenyl moiety was computationally developed and evaluated. All of the synthesized thiazolidin-4-one derivatives have their chemical structures characterized using a variety of methods, including nuclear magnetic resonance (NMR) (^{1}H and ^{13}C), high-resolution mass spectrometry (HRMS), and Fourier transform infrared (FTIR) radiation. A human glioblastoma cancer cell line (LN229) was used to investigate the purified derivatives' antiglioma cancer efficacy. By using the MTT, colony formation, and tunnel tests, respectively, the in vitro cytotoxic and apoptotic effects of these compounds were assessed. Thiazolidin-4-one derivatives **5b**, **5c**, and **5e** were discovered to have the best efficacy against glioblastoma cells out of all of these compounds. The derivatives **5b**, **5c**, and **5e** were determined to have respective IC_{50} values of 9.48, 12.16, and 6.43 g/mL. Computation results showed that the bioactivity evaluations of the compounds were quite significant. The bridging −NH group forms a hydrogen bond with Glu 260 of synthesized derivatives **5b**, **5c**, **5d**, **5e**, and **5h**. The vast majority of freshly developed compounds obeyed Lipinski's rule of five, which is in line with the results that the ADMET model predicted. Additionally, molecular docking evaluation and molecular dynamics simulation investigations against the proteins AURKA and VEGFR-2 were conducted for the synthesized compounds to incorporate both in silico and in vitro data. The findings revealed that almost all of the compounds had considerable binding to AURKA and VEGFR-2 residues, with binding affinities ranging from −9.8 to −7.9 kcal/mol. Consequently, the results of the biological investigations and the docking scores demonstrated that thiazolidinone molecule **5e** containing 4-chlorophenyl substituent may be considered as a potential moiety for glioblastoma cancer treatments.

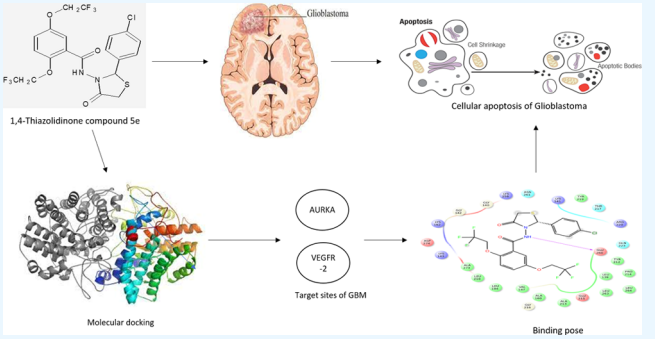

1. INTRODUCTION

A wide variety of malignancies are collectively termed cancer. These tumors are often distinguished by unchecked cellular growth and proliferation, uncontrolled cell migration, and the spread of organs and tissue.[1,2] When various regulatory, signaling, and apoptotic pathways are interfered with a variety of stimuli, a normal cell may develop tumors.[3] Carcinogenic cells mostly exhibit highly unregulated cellular proliferation as a distinguishing trait.[4]

The second most common cause of neurological disease-related death is central nervous system (CNS) malignancies.[5] Most intracranial tumor adults are gliomas, with glioblastoma multiform (GBM) having the worst prognosis and being the most frequent. It is very challenging to properly treat GBMs, which are grade IV gliomas, because of their rapid rate of proliferation and infiltrative growth pattern, which make them resistant to the medications that are currently being utilized.[6,7] Chemotherapy, radiation therapy, and the alkylating medication Temozolomide (TMZ), which results in DNA damage and cell death, are the current standards of care for the treatment of gliomas.[6,7] The most crucial aspect of tumor treatment is radiotherapy, which extends patient survival by 3−4 months for a period of 7−12 months. However, the survival increases from an average of 12.1−14.6 months when adjuvant TMZ is used.[8,9]

Today's cancer research is centered on developing novel, more efficient treatment modalities, such as "targeted" therapy, which focuses on a specific biochemical target or class of targets in cancer cells.[10,11] Therefore, developing new

Received: June 29, 2023
Accepted: September 29, 2023
Published: November 10, 2023

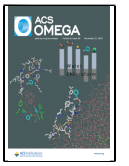

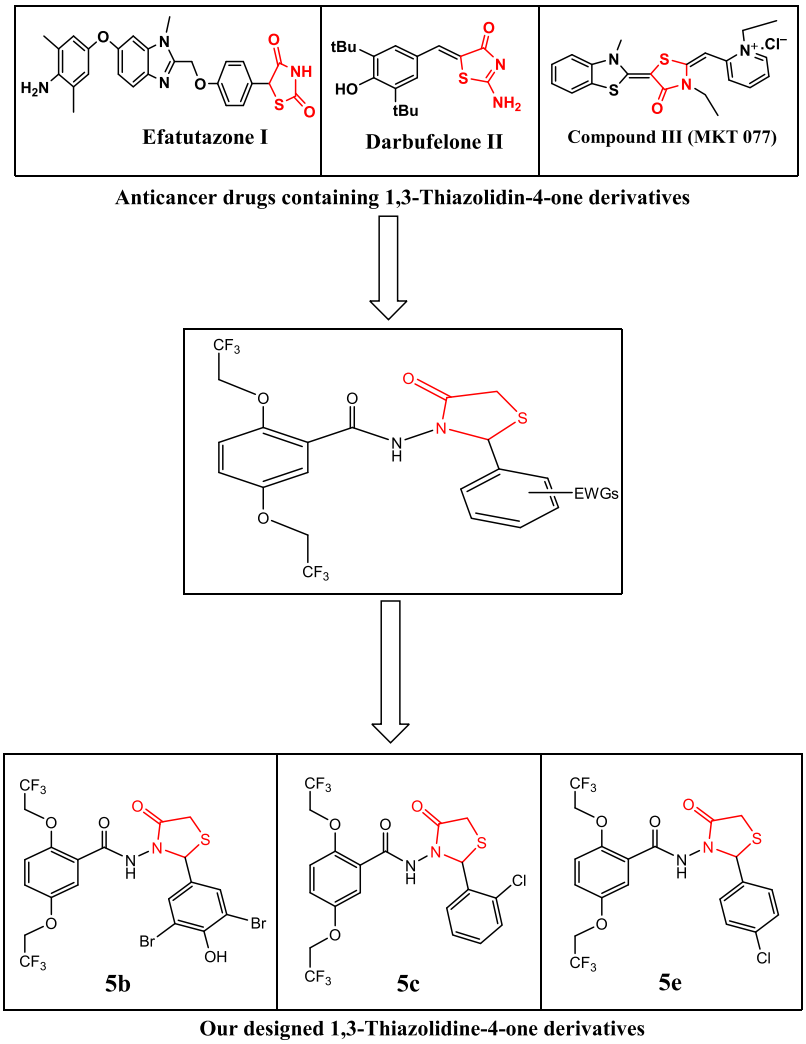

Figure 1. Design strategy for 2,5-bis(2,2,2-trifluoroethoxy)benzamide-1,3-thiazolidin-4-one hybrids.

anticancer drugs in medicinal chemistry that are selectively directed toward cancer cells is a fascinating application field.

The Aurora kinase family of enzymes is significant because it controls various facts of cellular division in mammalian cells, which includes Aurora A, B, and C. Failure to maintain a constant chromosomal content, a condition that can aid in tumorigenesis, has been linked to the dysfunction of these kinases.[12,13] Furthermore, Aurora-A is frequently carcinogenic and is increased in several tumor types. The therapeutic inhibition of these kinases, on the other hand, has shown its abilities in the treatment of cancer, probably because of their crucial roles during cell division.[14,15]

Another innovative target is VEGFR-2. Biological and preclinical data suggest that blocking VEGFR-2 may be an effective strategy to stop tumor-induced angiogenesis.[16,17] A significant VEGF-signaling effector is the VEGF receptor 2 (VEGFR-2), which is produced by the tumor as well as endothelial cells to boost both the autocrine and paracrine effects of VEGF -A signaling.[18] The overexpression of some VEGF ligands, such as VEGF-C and VEGF-D, is linked to the course of disease in a variety of solid tumors.[19]

Heterocyclic structures with nitrogen and sulfur are a well-known family of molecules that offer many opportunities for the synthesis of novel chemical compounds with physiological effects.[1,2] The study of 1,3-thiazolidin-4-ones, which are heterocyclic nuclei with sulfur, nitrogen, and a carbonyl group in the first and third positions, has expanded significantly in recent years.[20] The agile and adaptable thiazolidinone scaffold has been utilized in a variety of accurate diagnostic medications.[4,21] It is generally known that the thiazolidinone molecule (a thiazolidine ring with a carbonyl group) exerts a wide range of biological functions, and this molecule is recognized as a potent moiety in drug discovery.[22] This moiety plays a special role in a wide range of pharmacological substances helping to develop and improve different anticancer drugs.[23,24]

Due to numerous biological features, including its ability to be anticancer,[21,24,25] anti-HIV,[26] anti-inflammatory,[27] antitubercular,[28,29] antidiabetic,[30] antimicrobial[31] and antioxidant,[32] the 1,3-thiazolidine-4-one derivatives scaffold, in particular, is receiving a lot of interest. Recent decades have seen an increase in the importance of research on 1,3-Thiazolidine-4-one derivatives for their anticancer activity on prostate, breast, ovarian, lung, colon, kidney, central nervous system cancer, leukemia, and melanoma cell lines for the creation of anticancer medicines.[33,34]

Utilizing the structural frameworks of previously reported compounds, multifunctional molecular hybrids have been developed. There are numerous therapeutics on the market that combine the thiazolidinone substructure with other

https://doi.org/10.1021/acsomega.3c04662
ACS Omega 2023, 8, 43596−43609

heterocyclic moieties. Examples include Efatutazone I, which is well known for its effectiveness in treating metastatic colorectal cancer,[35] and Darbufelone II, which acts as a dual COX-2/5-LOX inhibitor on colon cancer cell growth and apoptosis.[36] A registered antitumor has also been recorded for Compound III (MKT 077)[37](Figure 1)

Given the foregoing, the goal of this research is to examine novel molecules that may serve as important anticancer agents. The primary goal of this work is to synthesize these heterocycles from acid hydrazide, various arene aldehydes, and mercaptoacetic acid, to use an in silico technique, and to assess their anticancer activity in GBM cells to prove them as an effective inhibitor of AURKA and VEGFR-2.

2. RESULTS AND DISCUSSION

2.1. Chemistry. Scheme 1 provides the reaction plan utilized to synthesize the title compound. The product of esterification of 2,5-bis(2,2,2-trifluoroethoxy)benzoic acid was utilized to synthesize the essential product, 2,5-bis(2,2,2-trifluoroethoxy)benzohydrazide (**3**). By condensing the relevant aldehydes with 2,5-bis(2,2,2-trifluoroethoxy)-benzohydrazide in an ethanol medium, the hydrazones (**4a-k**) were synthesized. The hydrazones and thioglycolic acid when refluxed with 1,4-dioxane yielded *N*-[2-(phenyl)-4-oxo-1,3-thiazolidin-3-yl]-2,5-bis(2,2,2-trifluoroethoxy)benzamide (**5a-k**).

The spectral assessment was ascertained using high-resolution mass spectrometry (HRMS), nuclear magnetic resonance (NMR), and infrared (IR) analyses (Table 1).

In the IR spectrum of *N*-[2-(3,4-dimethyl phenyl)-4-oxo-1,3-thiazolidin-3-yl]-2,5-bis(2,2,2-trifluoroethoxy)benzamide (**5d**), for −NH, the band was observed at 3398 cm^{-1}. The Ar−CH group showed a band at 3083 cm^{-1}. The CH band was found at 2918 cm^{-1}. The carbonyl absorption band of the thiazolidine ring was seen at 1717 cm^{-1}. A stretching vibration of the aromatic C−C bond was noticed at 1588 cm^{-1}. The band appeared at 1224 cm^{-1} due to the stretching vibration of C−O−C.

In addition, proton NMR showed a multiplet at δ 4.0−4.38 integrating for four protons, which was detected in the ^{1}H NMR spectra of compound 5d for the CH_2 group of the trifluoroethoxy group linked to the parent moiety. The CH_2 protons of the thiazolidine cycle were detected as a singlet at δ 3.7−3.9. The CH proton of the thiazolidine ring is responsible for a singlet at δ 5.95. The dimethyl groups showed resonance at δ 2.24 and 2.25. The signals are due to NH protons observed in the region of δ 8.89. The 6 protons of the benzene ring appeared as a multiplet at δ 6.84−7.68. Similarly, in the ^{13}C NMR spectrum of the compound, the dimethyl groups showed peaks at δ 19.4 and 19.6. The thiadiazoline CH_2 resonated at δ 30.1. The thiadiazoline CH resonated at δ 62.78. The CH_2 of the trifluoroethoxy group showed a peak at δ 66.1−67.6. The carbonyl carbon of the thiazolidine ring gave a peak at δ 162.6. The carbonyl carbon attached to NH gave a peak at δ 169.6. Additionally, the HRMS spectrum of this molecule revealed the molecular ion peak at m/z 551.0229 $[M + Na]^+$, which is compatible with the molecular formula = $C_{22}H_{20}F_6N_2O_4S$.

2.2. In Silico Studies. To screen the compounds, the binding energy and stable binding poses of drug molecules were anticipated. A two-dimensional (2D) ligand interaction diagram of 1,3-thiazolidine-4-one derivatives with (a) AURKA and (b) VEGFR-2 is shown in Figure 2. According to docking studies, the main variables affecting the interactions are hydrophobic and π-stacking interactions. For both AURKA

Scheme 1. Synthetic Route and Structures for Compounds 5a-k[a]

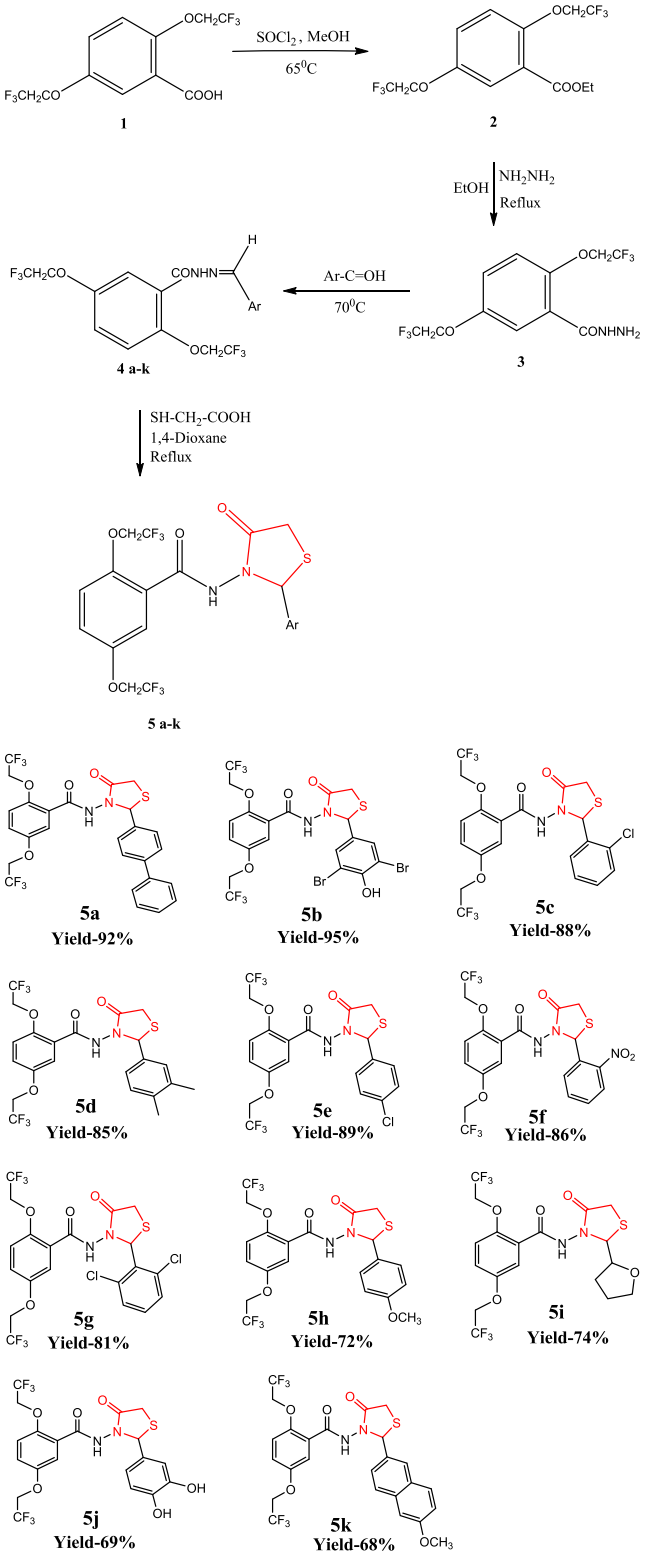

[a]Ar = 2-chlorophenyl, biphenyl, 3,5-dibromo-4-hydroxy phenyl, 3,4-dimethyl phenyl, 4-chlorophenyl, *m*-NO_2 benzaldehyde, 2,6-dichlor-ophenyl,4-methoxyphenyl, furfural, 3,4-dihydroxy phenyl, 6-methoxy naphthyl.

https://doi.org/10.1021/acsomega.3c04662
ACS Omega 2023, 8, 43596−43609

Table 1. Molecular Structure Data of Compounds 5a−k

compound. no	Ar	mol·wt	M.F	m.p (°C)	yield (%)
5a	biphenyl	570.5	$C_{26}H_{20}F_6N_2O_4S$	115−117	92
5b	3,5-dibromo-4-hydroxy phenyl	668.1	$C_{20}H_{14}Br_2F_6N_2O_5S$	172−173	95
5c	2-chlorophenyl	528.8	$C_{20}H_{15}ClF_6N_2O_4S$	102−104	88
5d	3,4-dimethyl	522.4	$C_{22}H_{20}F_6N_2O_4S$	142−144	85
5e	4-chlorophenyl	528.8	$C_{20}H_{15}ClF_6N_2O_4S$	111−113	89
5f	*m*-NO_2	539.4	$C_{20}H_{15}F_6N_3O_6S$	127−129	86
5g	2,6-dichlorophenyl	563.2	$C_{20}H_{14}Cl_2F_6N_2O_4S$	116−117	81
5h	4-methoxyphenyl	524.4	$C_{21}H_{18}F_6N_2O_5S$	106−108	72
5i	furfural	484.3	$C_{18}H_{14}F_6N_2O_5S$	121−123	74
5j	3,4-dihydroxy phenyl	526.4	$C_{20}H_{16}F_6N_2O_6S$	118−121	69
5k	6-methoxy naphthyl	574.4	$C_{25}H_{20}F_6N_2O_5S$	122−125	68

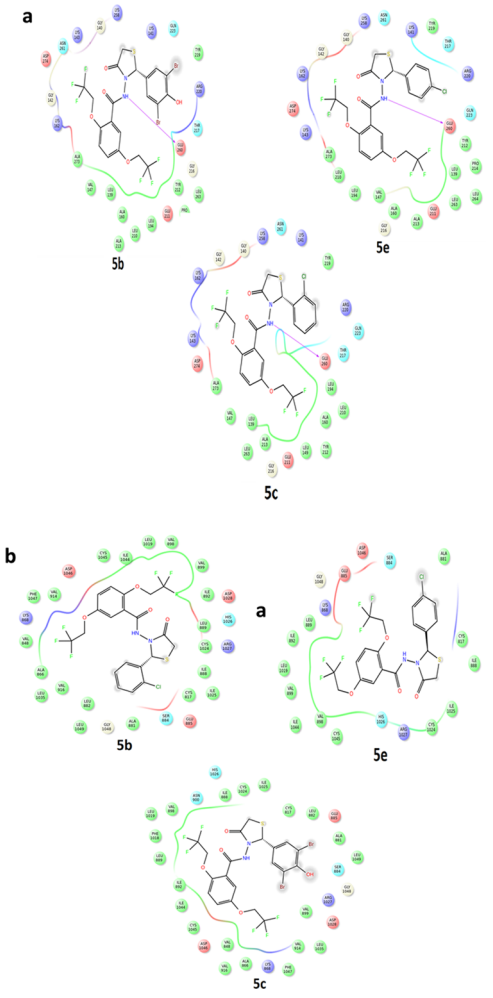

Figure 2. 1,3-Thiazolidine-4-one derivatives with (a) AURKA and (b) VEGFR-2:2D ligand interaction diagram.

and VEGFR-2, none of the molecules exhibited a strong tendency to create hydrogen bonds. The 1,3-thiazolidine-4-one derivative docking study-derived binding affinities are given in Table 2. Comparing 1,3-thiazolidine-4-one derivatives to Temozolomide (−5.7 and −5.9 kcal/mol), the maximum binding affinities were found for 1,3-thiazolidine-4-one derivatives with AURKA and VEGFR-2, respectively, in the vicinity of −9.8 to −8.0 and −9.4 to −7.9 kcal/mol.

2.2.1. AURKA. The interactions between the drug molecule and kinase enzyme are mainly noncovalent in nature, which are mainly the amino acid residues from Gly 140 to Asp 274 that

Table 2. 1,3-Thiazolidine-4-one Derivatives Binding Affinities (in kcal/mol) to AURKA and VEGFR-2

	binding affinity with (kcal/mol)	
compound	AURKA	VEGFR-2
temozolomide	−5.7	−5.9
1,3-Thiazolidine-4-one Derivatives		
5a	−9.8	−8.2
5b	−9.0	−8.7
5c	−8.9	−9.0
5d	−9.2	−8.1
5e	−8.7	−7.9
5f	−8.0	−9.4
5g	−8.5	−9.2
5h	−8.6	−8.7

cover the kinase's binding pocket. Most of the interactions between the molecules and residues Leu 273, Leu 263, Val 147, Leu 164, Leu 149, and Ala 160 are hydrophobic. The bridging −NH group of the synthesized derivatives **5b**, **5c**, **5d**, **5e**, and **5h** forms a hydrogen bond with Glu 260. The carbonyl group of the five-membered ring in **5a** and bridging carbonyl in **5f** form hydrogen bonds with the residues Lys 141 and Lys 143 respectively. The aromatic $\pi-\pi$ stacking interactions demonstrated by 1,3-thiazolidine-4-one derivative with AURKA are given in Table 3. The parameters for the interactions of

Table 3. $\pi-\pi$ Aromatic Interactions between AURKA and the 1,3-Thiazolidine-4-one Derivatives

compounds	residues	distance	angle	type
5a	Phe 144	6.35	83.26	edge-to-facee
	Trp 277	6.69	58.71	edge-to-face
5b	Tyr 219	5.70	70.50	edge-to-face
5c	Tyr 219	4.96	71.59	edge-to-face
5d	Tyr 219	6.37	66.84	edge-to-face
5e	Tyr 219	5.71	86.82	edge-to-face
5f	Phe 144	6.01	84.11	edge-to-face
	Trp 277	5.66	45.23	face-to-face
5g	Tyr 219	5.76	81.22	edge-to-face
5h	Tyr 219	5.94	71.94	edge-to-face

aromatic $\pi-\pi$ stacking are 4.5−5.5 Å for distance and 0−90° for the angle between normal vectors of two rings. It is clear that at a constant distance of around 5−6 Å, the compounds prefer edge-to-face contact to face-to-face interactions with the AURKA amino acid residues.

https://doi.org/10.1021/acsomega.3c04662
ACS Omega 2023, 8, 43596−43609

Further validation of the docking data was provided by 100 ns molecular dynamics simulations. Two compounds, **5e** (most active) and **5h** (moderately active), were chosen from the series to investigate how ligands behave dynamically at protein-binding locations. Figure 3 shows the RMSD profile as well as

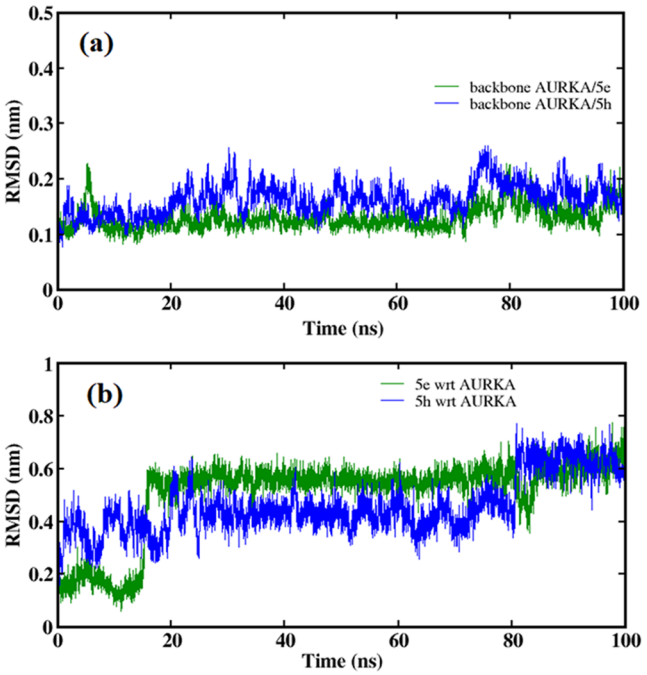

Figure 3. RMSD profiles of (a) backbone atoms in complexes with AURKA and (b) ligands concerning AURKA over 100 ns of simulation.

the backbone atoms concerning protein. It is conceivable that the conformation of the residues in the kinase's binding pocket was altered by the ligand binding. Because the protein fluctuations in the AURKA/**5h** complex are higher than those in the AURKA/5e complex, the mobility of active ligand **5e** is high with the kinase backbone with an average RMSD of 0.6 nm after 20 ns. The compound **5h** showed stable movements up to 80 ns, which further changed the binding geometry after 81 ns. Thus, it may be said that complex **5e** demonstrated stronger binding pocket stability than complex **5h**.

The ligand at the binding pocket was discovered to be stabilized via hydrogen-bond interactions, just like $\pi-\pi$ interactions. The results from molecular docking are supported by the average single hydrogen-bond contact being steady over the course of the 100 ns simulation (Figure 4). Hydrogen bonds could form between several residues, which are not seen in docking experiments since the ligand was able to adopt a favorable conformation at the pocket. Molecule **5e** demonstrated three interactions involving hydrogen bonds with residues Glu 260, Asn 261, and Lys 141, with Glu 260 making a greater contribution to stability than the other residues. The lower hydrogen-bonding occupancy is observed for the moderately active compound (Table 4).

Table 4. Occupancy of Hydrogen Bond between the Residues of Amino Acids and the Ligand in the Kinase Binding Pocket

ligand	hydrogen-bond occupancy (%)	
5e	**5e** (H) --- 260Glu (O)	14.0
	261Asn (H) --- **5e** (O)	6.5
	141Lys (H) --- **5e** (O)	9.9
5h	141Lys (H) --- **5h** (O)	25.1

2.2.2. VEGFR-2. Similar to how kinase enzymes interact with substances, the interactions of VEGFR-2 with treatment candidates were primarily hydrophobic in nature. The interactions are mostly confined to the region of the receptor's binding site, which consists of the amino acid residues from His 816 to Leu 1049. Most of the interactions between the bulky groups in the molecule and the amino acid residues, such as Cys 817, Ala 866, Val 848, Ala 881, Leu 882, Ile 888, Leu 889, Ile 892, Val 898, Val 916, Leu 1019, Cys 1024, Ile 1025, and Leu 1049, were hydrophobic. Only two of these derivatives, compounds **5d** and **5f**, demonstrated hydrogen-bonding interactions with residues Ile 1025 and Arg 1027, respectively. Table 5 lists the interactions between 1,3-thiazolidine-4-one derivatives and VEGFR-2 that exhibit $\pi-\pi$ stacking. The majority of 1,3-thiazolidine-4-one derivatives are shown to interact weakly face-to-face with the residues His 1026 and Phe 1047 at a distance around 6−9 and 8.6−9.8 Å, respectively. At the binding pocket, compound **5d** typically forms weak edge-to-face interactions with His 816. Unlike other compounds, **5f** prefers to form a stable edge-to-face interaction with His 1026 at a distance of 4.77 Å. The compounds **5g** and **5h** do not favor $\pi-\pi$ interactions, possibly due to the unfavorable ligand orientation.

Based on the experimental observations, the compounds **5e** (active) and **5h** (moderately active) were selected to learn the ligand's dynamic behavior at the VEGFR-2 binding site.

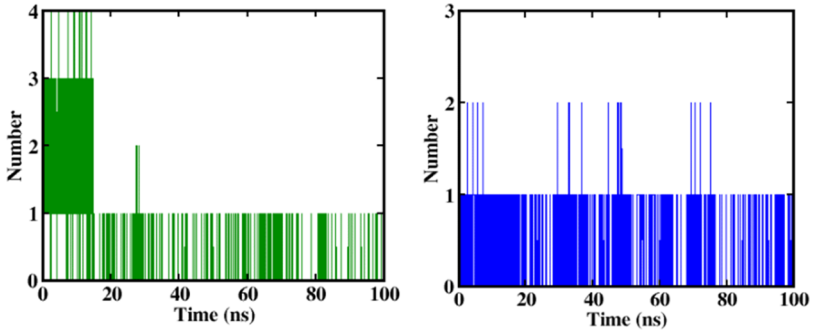

Figure 4. Representation of a number of hydrogen bonds established throughout the simulation at 100 ns. The plot shows the kinase complex with **5e** (green) and **5h** (blue).

https://doi.org/10.1021/acsomega.3c04662
ACS Omega 2023, 8, 43596−43609

Table 5. $\pi-\pi$ Aromatic Interactions between VEGFR-2 and the 1,3-Thiazolidine-4-one Derivative

compounds	residues	distance	angle	type
5a	His 1026	8.97	48.11	face-to-face
	Phe 1047	9.83	50.45	face-to-face
5b	His 1026	7.35	54.95	face-to-face
	Phe 1047	8.99	36.58	face-to-face
5c	His 1026	7.76	55.62	face-to-face
	Phe 1047	8.62	41.54	face-to-face
5d	His 816	10.73	88.66	edge-to-face
	His 1026	6.16	40.80	face-to-face
5e	His 1026	9.22, 6.28	45.56, 47.61	face-to-face
	Phe 1047	9.76	47.73	face-to-face
5f	His 1026	4.77	66.02	edge-to-face

Concerning the protein, the backbone atoms of VEGFR-2 and its ligand are represented by their RMSD profiles in Figure 5.

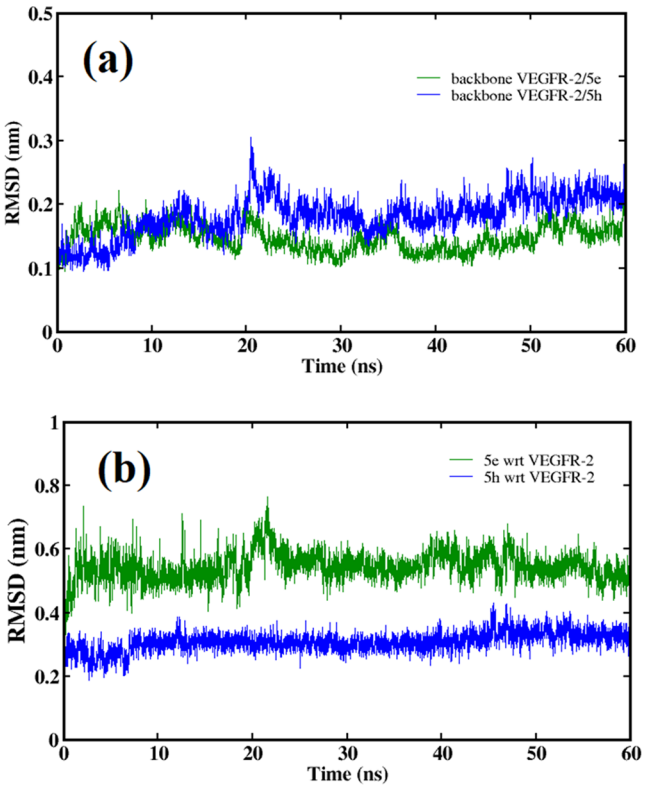

Figure 5. RMSD profiles of (a) backbone atoms in VEGFR-2/ligand complexes and (b) ligand relative to VEGFR-2 over the course of 60 ns simulations.

The revelation that protein fluctuations are larger in the VEGFR-2/**5h** complex than in the VEGFR-2/**5e** complex alludes to a change in the conformation of residues in the binding pocket following the ligand interaction. Ligand movements cope well with protein movement. It is observed that compound **5e** stabilizes at the VEGFR-2 binding pocket at a higher RMSD value compared to compound **5h**. In addition, the numerous hydrogen bonds that occur between the ligands and the VEGFR-2 binding site help to explain the stability of the molecule. The compound **5e** was found to have stable hydrogen bond interactions with the residue Arg 1027 throughout the simulation (Figure 6). The hydrogen-bond occupancy for compound **5h** is much lower, suggesting an unfavorable ligand orientation at the binding site (Table 6). Thus, it can be concluded that **5e** is the favorable drug candidate to bind the VEGFR-2 binding site through hydrogen-bonding interactions and $\pi-\pi$ interactions than **5h**.

2.2.3. ADME Toxicity Prediction. Metabolism, distribution, adsorption, excretion, as well as toxicity are some of the pharmacokinetic (PK) characteristics that were determined using the Swiss ADME web application. Using a series of protocols, the synthetic molecule's drug-likeness, potency, and bioavailability were anticipated as provided in Table S.1 (Supporting Information). Except for compounds **5a** and **5g**, all of the compounds adhered to Lipinski's rule of five. Because every synthesized compound has a molecular weight of more than 500 g/mol, these substances are membrane-permeable. For all of the compounds, it was discovered that the dipole moment, rotatable bonds, several hydrogen bond acceptors, and several hydrogen-bond donors were all within the acceptable ranges of 1.0−12.5 debye, 0−15, 0.0−6.0, and 2.0−20.0, respectively. The cumulative chemical cell permeability value, or the polar surface area, ranges from 93.17 to 138.99 Å^2, indicating good oral availability. The BBB assessment makes it clear that substances do not effectively cross the blood−brain barrier (BBB) if the polar surface area is less than <60 Å^2. The projected PSA values are less than 139 Å^2, which indicates that the molecules have favorable intestine absorption characteristics. Molar refractivity tells the individual ion's electronic polarizability and how they interact in solutions. The synthesized molecules have refractive values ranging from 114.02 to 134.44 m^3/mol. Compound **5a** has a refractivity value over the allowable range. Except for **5a** and **5g**, the projected ADMET features imply that the compounds can be useful therapeutic molecules.

2.3. Pharmacology. *2.3.1. Anticancer Cytotoxic Study.* The MTT assay was used to examine the cytotoxic effects of all newly synthesized 1,3-thiazolidine-4-one derivatives on LN229 cells of glioblastoma. For 48 h, newly synthesized drugs were exposed at a concentration of 0, 5, 10, 15, 20, and 25 μm as shown in Figure 7. The IC_{50} values and the percentage of cell death for all freshly synthesized substances are given in Table 7. In this regard, compounds containing side chains such as 3,5-dibromo-4-hydroxy (**5b**), 2-chloro (**5c**), and 4-chloro (**5e**) had only 41.2, 32.5, and 24.2% of cell viability, respectively, ensuring that they had the highest cytotoxic effects, as shown in Figure 8(A). The compounds without halogen substituents such as biphenyl (**5a**) and 4-methoxy (**5h**) have shown the least activity and moderate to less activity. Figure 8(B) illustrates the IC_{50} value. This confirms that compounds such as **5b**, **5c**, and **5e** cause 58.75, 67.48, and 75.75% of cell death, which consist of 9.48, 12.16, and 6.43 μm as IC_{50} concentrations, respectively.

2.3.2. Colony Formation Assay. The current study sought to determine whether the cytotoxic profiles of individual drugs in MTT influenced the relevant changes in the biological processes of the LN229 cells. As a result, LN229 cells were exposed to 10 μm and a maximum of 25 μm of metal (as selected from the MTT assay) to compare the efficiency of compounds **5b**, **5c**, and **5e** to limit the proliferation and colony formation. The capacity of a single cell to form many colonies is restricted by all of the screened compounds at 25 μm, as shown in Figure 9(A). Furthermore, **5e** has been shown to have the greatest mobility restriction and cytotoxic inhibition; this is followed by **5c** and **5b**, all three of which have significant cell proliferation inhibition capabilities.

https://doi.org/10.1021/acsomega.3c04662
ACS Omega 2023, 8, 43596−43609

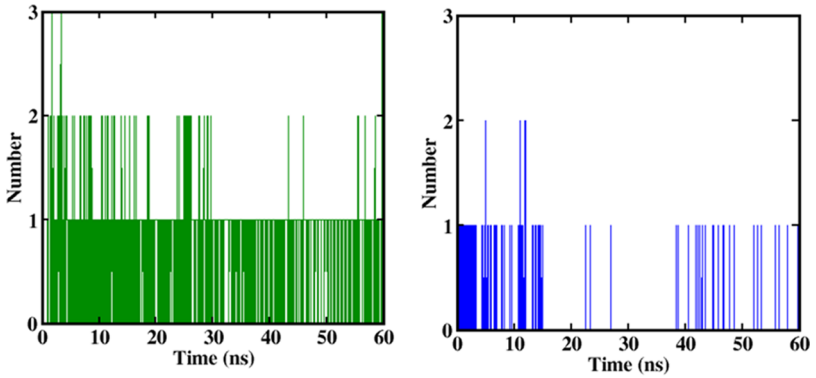

Figure 6. Hydrogen bonds generated on average during a 60 ns simulation. The VEGFR-2 complex is shown on the plot as **5e** (green) and **5h** (blue).

Table 6. Occupancy of Hydrogen Bond between the Residues of Amino Acid and the Ligand in the Binding Pocket of VEGFR-2

ligand	hydrogen-bond occupancy (%)	
5e	1027 Arg (H11) --- **5e** (O)	85.9
	1027 Arg (H11) --- **5e** (O1)	1.1
	816 His (H) --- **5e** (O)	0.4
5h	1046 Asp (H) --- **5h** (O)	1.1
	1046 Asp (H) --- **5h** (N)	0.6
	1026 His (HE2) --- **5h** (O)	0.3

2.3.3. Tunel Assay. The TUNEL assay will aid in identifying the apoptotic cellular fragmented DNA hydroxyl group for further validation of the cytotoxic effects of the screened compounds. To evaluate the molecular effectiveness of the screened compounds, glioblastoma cell lines were exposed to compounds **5b**, **5c**, and **5e** for roughly 48 h. DNA strand breaks (DSBs), which are produced when nuclear DNA is extensively fragmented, were found in the treatment groups by using green (FITC)-labeled fluorochromes (Figure 10). Cells from groups of positive controls were exposed to the DNase enzyme, whose DNA frequently exhibits high levels of CFTC expression. The DNA of the negative control, in contrast, exhibits no fluorescence since it was untouched. In comparison to the negative control, the relative FITC expression of the screened compounds was examined. These findings demonstrate the potential anticancer capabilities of the tested compounds (**5b**, **5c**, and **5e**) at the molecular level.

3. CONCLUSIONS

With comparatively good yields, a new series of substituted 1,3-thiazolidinone compounds were synthesized. The synthesized compounds **5a-h** were the subject of in silico research. All

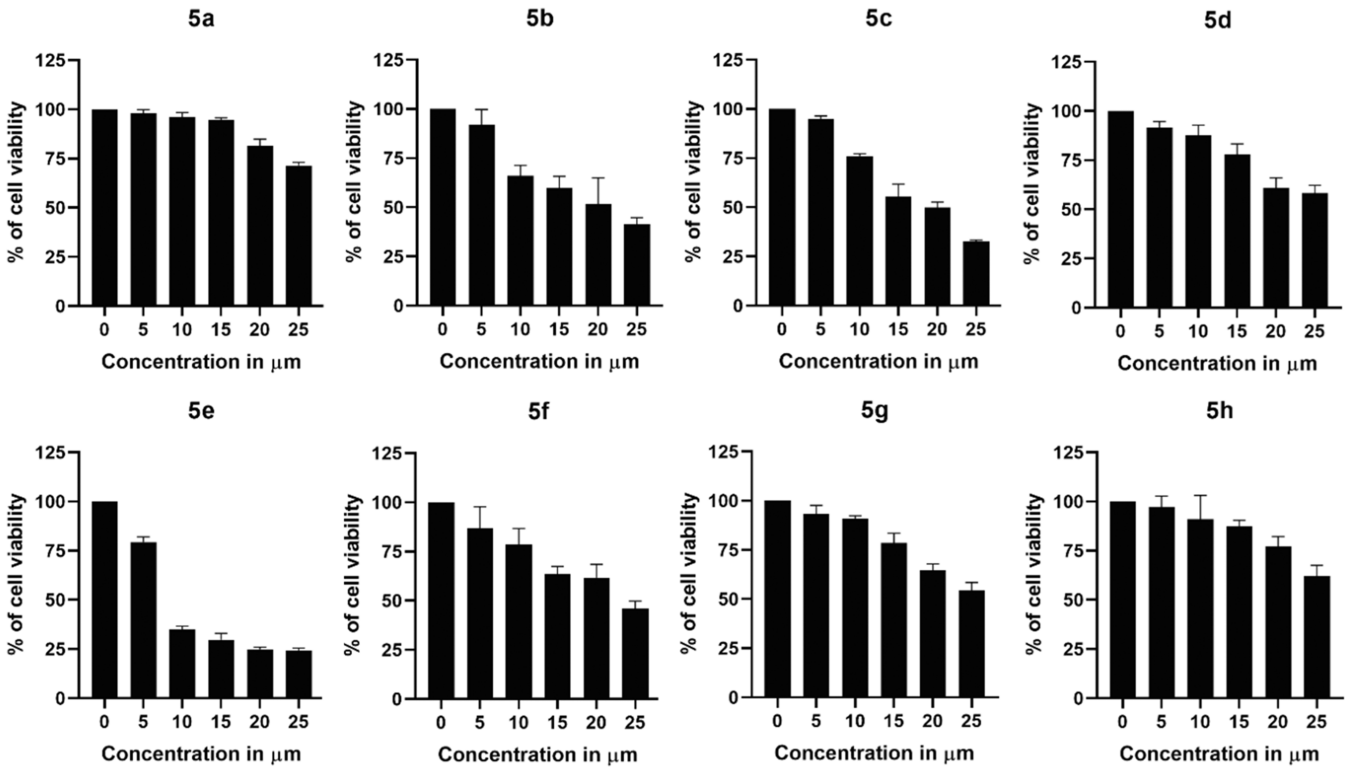

Figure 7. Data on the screened compounds' cell viability.

https://doi.org/10.1021/acsomega.3c04662
ACS Omega 2023, 8, 43596−43609

Table 7. IC_{50} Values and the Percentage of Cell Death for All of the Newly Synthesized Molecules

1,3-thiazolidine-4-one derivatives	Ar	IC_{50} value in μM	% of cell death at 25 μM	% of cell viability at 25 μM
5a	biphenyl	18.12	27.50	72.49
5b	3,5-dibromo-4-hydroxy phenyl	9.48	58.75	41.24
5c	2-chlorophenyl	12.16	67.48	32.51
5d	3,4-dimethyl	12.94	41.91	58.08
5e	4-chlorophenyl	6.43	75.75	24.24
5f	*m*-NO_2	10.53	54.02	45.92
5g	2,6-dichlorophenyl	14.7	45.87	54.12
5h	4-methoxyphenyl	16.4	37.56	62.43

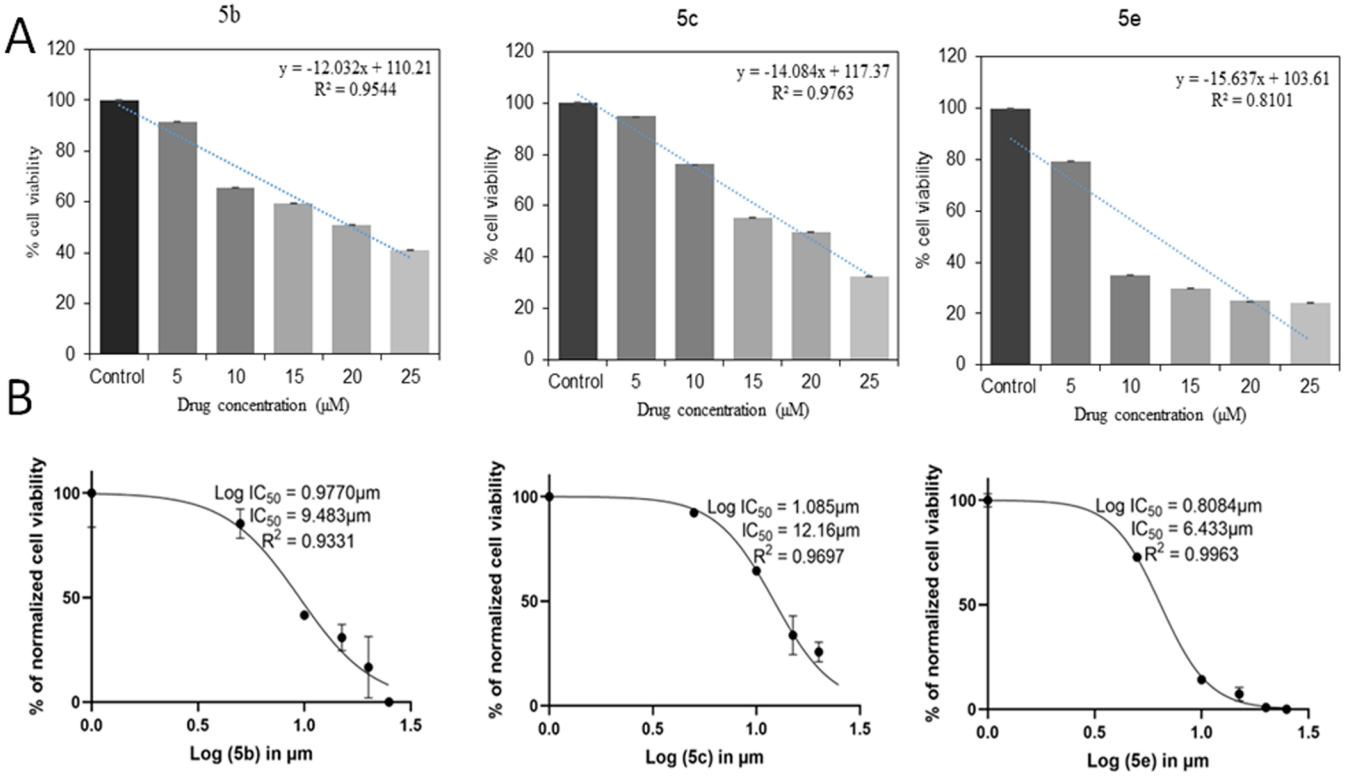

Figure 8. (A) Cell viability percentage and (B) Hill plot curve showing the IC_{50} for the 1,3-thiazolidine-4-one derivatives that were tested.

of the synthesized compounds had relatively lower binding energies than the conventional medication Temozolomide, according to in silico studies, and may be suitable as inhibitors of Aurka and VEGFR-2 of glioblastoma. The bridging −NH group of the synthesized derivatives, **5b**, **5c**, **5d**, **5e**, and **5h** forms a hydrogen bond with Glu 260. The results from docking were confirmed by the molecular dynamic simulation of the highly active molecule with the enzymes, which also demonstrated the stability of the protein−ligand complex stability. According to simulation data, hydrogen-bond interactions play an identical role in ligand stability at the binding pocket. Most synthetic compounds follow Lipinski's rule of five, which is consistent with the predictions of the ADMET model, which shows them as a good drug candidate for therapeutic use. The docking outcomes were also connected to biological research. The efficiency of the newly synthesized 1,3-thiazolidin-4-one moiety as an AURKA and VEGFR-2 inhibitor was investigated in vitro. Therefore, the potential for developing these 1,3-thiazolidinone derivatives as effective anticancer drugs has been expanded as a result of our investigation. Additionally, the trifluoroethoxy-group-containing synthetic compounds were further investigated for their in vitro cytotoxic effects on LN229 glioblastoma cell lines. Likewise, among the newly synthesized derivatives, compounds with the electron-withdrawing substituents 3,5-dibromo-4-hydroxy (**5b**), 2-chlorophenyl (**5c**), and 4-chlorophenyl (**5e**) showed strong cytotoxic effects in the MTT experiment. This was further supported by restricting the rate at which colonies grow, as well as by triggering cellular death (tunnel assay) at a concentration of 25 m.

Finally, the biological inquiry findings line up with the in silico results, indicating that the synthesized molecules may be effective at inhibiting glioblastoma's Aurka and VEGFR-2. The halogen-substituted **5b**, **5c**, and **5e** compounds have shown excellent results. By causing cell death, the electron-withdrawing 4-chloro-substituted hit compound **5e** became a highly effective anticancer drug.

4. MATERIALS AND METHODS

4.1. Synthesis. Melting points were investigated by using the open capillary technique; the outcomes were not corrected. The IR spectra were generated by the KBr pellet technique and recorded using a Bruker FTIR-4100 spectrophotometer. The compounds were analyzed using a Joel (400 MHz) instrument

https://doi.org/10.1021/acsomega.3c04662
ACS Omega 2023, 8, 43596−43609

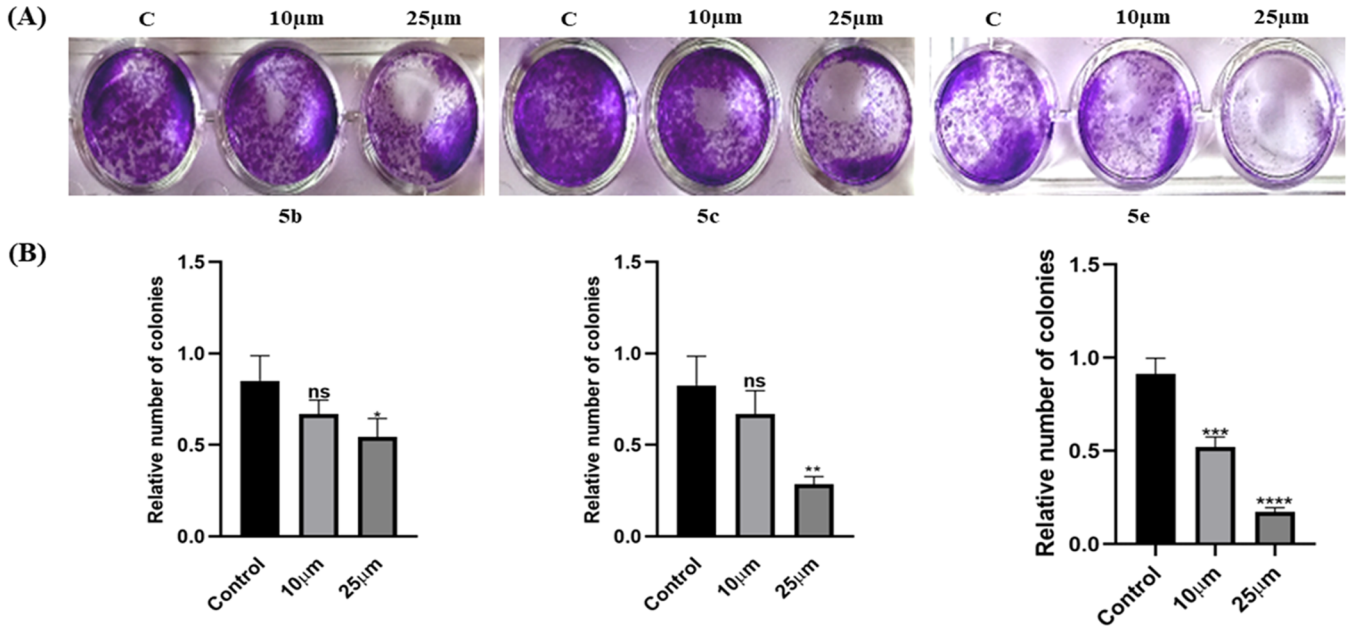

Figure 9. Colony formation tests were used to calculate the relative rate of proliferation of the LN229 brain cancer cell line. (A) Typical illustrations of the colony-forming assay. (B) Calculation of the LN229 cell colony formation rate. Results from three different experiments are presented as the mean and standard deviation. ns, not significant *P < 0.05, **P < 0.01, ***P < 0.001, ****P < 0.0001 vs respective control group.

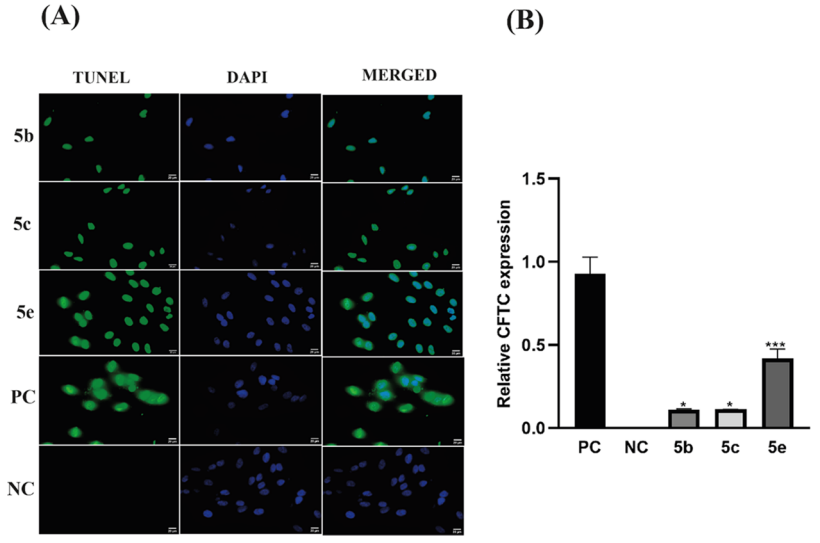

Figure 10. Results of the TUNEL assay after 48 h of treatment. (A) Quantity of TUNEL-positive cells was noticeably increased in compounds **5b**, **5c**, and **5e** compared to the negative control group (original magnification 20 μm). The use of DAPI staining served as a counterstain. (B) Comparison of the relative quantification of **5b**, **5c**, and **5e**'s FITC (green) expression to the negative control. The report of the standard and mean deviation of two identical experiments are represented (*P < 0.05, **P < 0.01, ***P < 0.001).

for ^{1}H NMR using TMS as an internal standard. The units of chemical shift readings are ppm or δ units. The mass spectra were recorded using an HRMS instrument (model name, Waters-Xevo G2-XS-QToF). Silica-gel-coated aluminum sheets (silica gel 60 F254), which were acquired from Merck, were used to conduct thin-layer chromatography (TLC) to track the development of the reaction. The synthesized compounds were purified by using reagents and solvents of commercial quality.

4.2. Procedure for the Synthesis of 2,5-Bis(2,2,2-trifluoroethoxy) benzohydrazide(3). 2,5-Bis(2,2,2-trifluoroethoxy)benzoic acid (20 g, 0.0628 mol) was dissolved in methanol (60 mL), and the slow addition of thionyl chloride (14.27 g, 0.12 mol) was done at 0−5 °C. The mass was slowly heated to 60−65 °C and maintained for 1 h to get 2,5-bis(2,2,2-trifluoroethoxy)benzoester (**2**). To monitor the reaction's development, TLC was checked. The mass is then distilled to eliminate unutilized thionyl chloride, then neutralized with 5% sodium bicarbonate, and extracted using ethyl acetate two times (40 mL each time). The product containing an organic layer is concentrated below 50 °C under vacuum to get the esterification product (Yield = 94%).

Further, 2,5-bis(2,2,2-trifluoroethoxy)benzoester (**2**) (15 g, 0.043 mol) and 85% hydrazine hydrate (5.3 g, 0.090 mol) were dissolved in absolute alcohol (25 mL) and refluxed the clear solution for 3 h. The reaction completion was examined using

https://doi.org/10.1021/acsomega.3c04662
ACS Omega 2023, 8, 43596−43609

TLC. Then, the reaction mass was distilled off to eliminate excess alcohol. The solid precipitated was filtered using a Buchner funnel, rinsed with precooled ethanol, and vacuum-dried at 55−65 °C (Yield is 94%).

4.3. General Process for Synthesizing Hydrazone 4a-k. 2,5-Bis(2,2,2-trifluoroethoxy)benzohydrazide (**3**) (1 g, 0.00301 mol) and an appropriate aldehyde (0.0033 mol) were mixed, and the combination was heated for 2 h at 70−75 °C in ethanol. Further reaction mass was slowly allowed to attain a temperature of 25 ± 5 °C and subsequently cooled to 0−5 °C. The precipitated solid was filtered over the Buchner funnel, washed using prechilled ethanol, and dried at 55−65 °C.

4.4. General Method for Synthesizing *N*-[2-(Phenyl)-4-oxo-1,3-thiazolidin-3-yl]-2,5-bis(2,2,2-trifluoroethoxy)benzamide (5a-k). Thioglycolic acid (0.01 mol) and **4a-k** (0.01 mol) were combined and refluxed in 1,4-dioxane solvent for 7−8 h. The progress of the reaction was tracked by TLC, and after that, the extra solvent was distilled off at 55−65 °C under decreased pressure; the concentrated residue was solubilized in ethyl acetate and then washed with sodium hydrogen carbonate solution (5%). The clear organic layer containing the product was collected and distilled to a minimum volume to separate the solid. The resulting solid product was separated by Buchner filtration and washed with hexane, and hot ethanol recrystallization was done to produce a pure product. The material was dried at 55−65 °C.

*4.4.1. N-[2-(4-Biphenyl)-4-oxo-1,3-thiazolidin-3-yl]-2,5-bis(2,2,2-trifluoroethoxy)benzamide (**5a**).* White microcrystals; mp 115−117 °C; IR (KBr) γ/cm^{-1}: 3398 (NH), 3069 (ArC−H), 2979 (C−H), 1672 (C═O of thiazolidinone), 1717 (C═O NH), 1264 (C−O−C); ^{1}H NMR ($CDCl_3$, 400 MHz): δ 8.91 (s, 1H, NH), 7.61 (d, J = 3.3 Hz, 1H, Ar−H), 7.47−7.54 (m, 4H, biphenyl ring 1), 7.38 (dd, J = 8.0 Hz, 4H, biphenyl ring 2), 7.29 (t, J = 7.3 Hz, 1H, biphenyl ring), 7.02 (dd, J = 9.1, 1H, Ar−H), 6.76 (d, J = 9.0 Hz, 1H, Parent Ar−H), 5.99 (s, 1H, CH of thiazole), 4.03−4.30 (m, 4H, CH_2CF_3), 3.76 (dd, J = 48.9, 15.9 Hz, 2H, CH_2 of thiazolidinone); ^{13}C NMR ($CDCl_3$, 100 MHz): δ 30.12 (CH_2 of thiazolidinone), δ 62.73 (CH of thiazolidinone), δ 65.75−67.28 (quartet, $^2J_{CF}$= 35.9 Hz,CH_2CF_3), δ 115.33,117.17,120.99 ($C_{9,10,11}$ of biphenyl), δ121.11−123.87-(quartet, $^1J_{CF}$= 264 Hz,CF_3-coupling), δ127.78,127.67,127.31,127.04 ($C_{2,6,8,12}$ of biphenyl), δ 128.98,128.82,128.01 ($C_{1,4,7}$ of biphenyl), δ 135.86 (C_3 of Ar), δ 140.20 (C_4 of Ar), δ142.57,(C_1 of Ar), δ 150.27 (C_6 of Ar), δ 162.71,153.05 ($C_{2,5}$ of Ar), δ 169.73 (C═O of thiazolidinone), δ 174.16 (C═O attached to NH); HRMS (ESI, m/z):593.0974 $[M + Na]^+$; calcd for $C_{26}H_{20}F_6N_2O_4S$: 570.5034; found 570.1077.

*4.4.2. N-[2-(3,5-Dibromo-4-hydroxy phenyl)-4-oxo-1,3-thiazolidin-3-yl]-2,5-bis(2,2,2-trifluoroethoxy)benzamide (**5b**).* White microcrystals; mp 172−173 °C; IR (KBr) γ/cm^{-1}: 3396 (NH), 3062 (ArC−H), 3031 (C−H), 1673 (C═O of thiazolidine), 1720 (C═O NH), 1285 (C−O−C); ^{1}H NMR ($CDCl_3$, 400 MHz): δ 8.85 (s, 1H, NH), 7.63 (d, 1H, Parent Ar−H), 7.45 (s, 2H, of substituted Ar−H), 7.07 (dd, J = 9.2, 3.3 Hz, 1H, Parent Ar−H), 6.79 (d, J = 9.0 Hz, 1H, Parent Ar−H), 6.03 (s, 1H, OH), 5.79 (s, 1H, CH of thiazolidinone), 4.19−4.36 (m, 4H, CH_2CF_3), 3.79 (d, J = 16.1 Hz, 2H, CH_2 of thiazolidinone); ^{13}C NMR ($CDCl_3$, 100 MHz): δ 30.01 (CH_2 of thiazolidine), δ 61.64 (CH of thiazolidine), δ 66.17−67.13 (quartet, $^2J_{CF}$ = 36 Hz,CH_2CF_3),δ 110.20,114.90 ($C_{2,6}$ of side chain Ar−H), δ 121−124(quartet, $^1J_{CF}$ = 276 Hz,CF_3-coupling), δ 121.66 (C_1 of side chain Ar), δ 122.27 (C_4 of Ar), δ 123.88 (C_6 of Ar), δ 124.40(C_1 of Ar), δ 131.61, 131.48 ($C_{2,5}$ of Ar), δ 150.23 (C_4 of side chain Ar−H), δ 153.02,150.44 ($C_{3,5}$ of side chain Ar−H), δ 162.86 (C═O of thiazolidine), δ 169.35 (NH−C═O); HRMS (ESI, m/z): 690.8768 $[M + Na]^+$; calcd for $C_{20}H_{14}Br_2F_6N_2O_5S$: 668.1989; found 667.8868.

*4.4.3. N-[2-(2-Chlorophenyl)-4-oxo-1,3-thiazolidin-3-yl]-2,5-bis(2,2,2-trifluoroethoxy)benzamide (**5c**).* White microcrystals; mp 102−104 °C; IR (KBr) γ/cm^{-1}: 3391 (NH), 3250 (ArC−H), 2992 (C−H), 1666 (C═O of thiazolidine), 1707 (C═O NH), 1285 (C−O−C); ^{1}H NMR ($CDCl_3$, 400 MHz): δ 9.02 (s, 1H, NH), 7.71 (d, J = 3.1 Hz, 1H, Parent Ar−H), 7.46 (dd, J = 7.5 Hz, 1H, Parent Ar−H), 7.29−7.39 (m, 3H, 3,5,6 of substituted Ar−H), 7.12 (dd, J = 9.0, 1H, Parent Ar−H), 6.86 (d, J = 9.0 Hz, 1H,4H of substituted Ar−H), 6.47 (s, 1H, CH of thiazolidinone), 4.32−4.44 (m, 4H, CH_2CF_3), 3.82 (t, J = 16.2 Hz, 2H, CH_2 of thiazolidinone); ^{13}C NMR ($CDCl_3$, 100 MHz): δ 29.64 (CH_2 of thiazolidine), δ 59.59 (CH of thiazolidine), δ 65.76−67.20. (quartet, $^2J_{CF}$ = 36 Hz,CH_2CF_3),δ 115.02,117.25,120.85,121.18 ($C_{3,4,5,6}$ of side chain Ar−H), δ 121.64,122.16,123.95,124.40(quartet, $^1J_{CF}$ = 276 Hz,CF_3-coupling), δ 127.69 (C_4 of Ar), δ 127.80 (C_3 of Ar), δ 130.15 (C_6 of Ar), δ 130.29 (C_1 of side chain Ar), δ 133.50 (C_2 of side chain Ar−H), δ 135.16 (C_1 of Ar), δ 152.99,150.23 ($C_{2,5}$ of Ar), δ 162.75 (C═O of thiazolidine), δ 169.79 (NH−C═O); HRMS (ESI, m/z): 551.0229 $[M + Na]^+$; calcd for $C_{20}H_{15}ClF_6N_2O_4S$: 528.8525; found 528.0332.

*4.4.4. N-[2-(3,4-Dimethyl phenyl)-4-oxo-1,3-thiazolidin-3-yl]-2,5-bis(2,2,2-trifluoroethoxy)benzamide (**5d**).* White microcrystals; mp 142−144 °C; IR (KBr) γ/cm^{-1}: 3441 (NH), 3023 (ArC−H), 2979 (C−H), 1684 (C═O of thiazolidine), 1725 (C═O NH), 1293(C−O−C); ^{1}H NMR ($CDCl_3$, 400 MHz): δ 8.89 (s, 1H, NH), 7.68 (d,1H, Parent Ar−H), 7.46 (dd, J = 7.5 Hz, 1H, Parent Ar−H), 7.29−7.39 (m, 3H, 3,5,6 substituted Ar−H), 7.12 (dd, J = 9.0, 1H, Parent Ar−H), 6.86 (d, J = 9.0 Hz, 1H,4H substituted Ar−H), 5.95 (s, 1H, CH of thiazolidinone), 4.21−4.38 (m, 4H, CH_2CF_3), 3.80 (t, J = 15.9 Hz, 2H, CH_2 of thiazolidinone), 2.25 (d, J = 2.2 Hz, 6H, 2 CH_3); ^{13}C NMR ($CDCl_3$, 100 MHz): δ 19.4,19.6 (2 CH_3), δ 30.1 (CH_2 of thiazolidine), δ 62.78 (CH of thiazolidine), δ 66.1−67.8. (quartet, $^2J_{CF}$ = 36 Hz,CH_2CF_3), δ 116.01,117.06 ($C_{3,4}$ of side chain Ar), δ 121.47,122.12,125.08 ($C_{2,5,6}$ of side chain Ar), δ 128.41 (quartet, $^1J_{CF}$ = 332 Hz, CF_3-coupling), δ 137.70 (C_1 of side chain Ar), δ 134.36 (C_4 of Ar), δ 130.17 (C_3 of Ar), δ 138.35 (C_1 of Ar), δ 134.36 (C_6 of Ar), δ 153.21,150.42 ($C_{2,5}$ of Ar), δ 162.63 (C═O of thiazolidine), δ 169.66 (NH−C═O); HRMS (ESI, m/z): 545.0966 $[M + Na]^+$; calculated for $C_{22}H_{20}F_6N_2O_4S$: 522.4606; found 522.1069.

*4.4.5. N-[2-(4-Chloro phenyl)-4-oxo-1,3-thiazolidin-3-yl]-2,5-bis(2,2,2-trifluoroethoxy)benzamide (**5e**).* White microcrystals; mp 111−113 °C; IR (KBr) γ/cm^{-1}: 3402 (NH), 3072 (ArC−H), 2945 (C−H), 1683 (C═O of thiazolidine), 1726 (C═O NH), 1291 (C−O−C); ^{1}H NMR ($CDCl_3$, 400 MHz): δ 8.91 (s, 1H, NH), 7.69 (d, 1H, Parent Ar−H), 7.35 (s, 4H, substituted Ar−H), 7.12 (dd, J = 9.0, 3.3 Hz, 1H, Parent Ar−H), 6.85 (d, J = 9.2 Hz, 1H, Parent Ar−H), 5.98 (s, J = 1.2 Hz, 1H, CH of thiazolidinone), 4.17−4.40 (m, 4H, CH_2CF_3), 3.80 (ddd, J = 50.6, 15.9, 1.2 Hz, 2H, CH_2 of thiazolidinone); ^{13}C NMR ($CDCl_3$, 100 MHz): δ 30.04 (CH_2 of thiazolidine), δ 62.35 (CH of thiazolidine), δ 66.17−67.23. (quartet, $^2J_{CF}$ = 34

https://doi.org/10.1021/acsomega.3c04662
ACS Omega 2023, 8, 43596−43609

Hz,CH_2CF_3), δ 115.11,117.28,120.85,121.12 ($C_{2,3,5,6}$ of side chain Ar), δ 123.89, 122.17, 121.64 (quartet, $^1J_{CF}$ = 277 Hz, CF_3-coupling), δ 124.411 (C_4 of Ar), δ 129.08 (C_3 of Ar), δ 130.15 (C_6 of Ar), δ 129.26 (C_1 of side chain Ar), δ 135.48 (C_1 of Ar), δ 135.57 (C_4 of side chain Ar), δ 153.06,150.24 ($C_{2,5}$ of Ar), δ 162.74(C═O of thiazolidine), δ 169.53 (NH−C═O); HRMS (ESI, *m*/*z*): 551.0229 $[M + Na]^+$; calcd for $C_{20}H_{15}ClF_6N_2O_4S$: 528.8525; found 528.0332.

*4.4.6. N-[2-(m-Nitrophenyl)-4-oxo-1,3-thiazolidin-3-yl]-2,5-bis(2,2,2-trifluoroethoxy)benzamide (**5f**).* White microcrystals; mp 127−129 °C; IR (KBr) γ/cm^{-1}: 3398 (NH), 3091(ArC−H), 2995 (C−H), 1677 (C═O of thiazolidine), 1721 (C═O NH), 1291 (C−O−C); ^{1}H NMR ($CDCl_3$, 400 MHz): δ 8.94 (s, 1H,NH), 8.30 (t, *J* = 1.9 Hz, 1H, 5H of substituted Ar−H), 8.24 (dq, *J* = 8.2, 1.1 Hz, 1H, 3H of substituted Ar−H), 7.79 (d, *J* = 7.7 Hz, 1H, Parent Ar−H), 7.70 (d, *J* = 3.3 Hz, 1H, Parent Ar−H), 7.60 (t, *J* = 7.9 Hz, 1H, 6H of substituted Ar−H), 7.14 (dd, *J* = 9.0, 3.3 Hz, 1H, 2H of substituted Ar−H), 6.84 (d, *J* = 9.2 Hz, 1H, Parent Ar−H), 6.08 (s, 1H, CH of thiazolidinone), 4.23−4.41 (m, 4H, CH_2CF_3), 3.86 (ddd, *J* = 39.4, 16.0, 1.3 Hz, 2H, CH_2 of thiazolidinone); ^{13}C NMR ($CDCl_3$, 100 MHz): δ 30.01 (CH_2 of thiazolidine), δ 62.20 (CH of thiazolidine), δ 66.18−66.95 (quartet, $^2J_{CF}$ = 36 Hz,CH_2CF_3), δ 114.68,117.37,120.53,121.32 ($C_{2,3,5,6}$ of side chain Ar), δ 122.32(quartet, $^1J_{CF}$ = 240 Hz,CF_3-coupling), δ 122.93 (C_4 of Ar), δ 130.17 (C_3 of Ar), δ 124.46 (C_6 of Ar), δ 133.72 (C_1 of Ar), δ 139.69 (C_1 of Ar), δ 148.59 (C_4 of side chain Ar), δ 153.02,150.17 ($C_{2,5}$ of Ar), δ 162.96 (C═O of thiazolidine), δ 169.54 (NH−C═O); HRMS (ESI, *m*/*z*): 562.0502 $[M + Na]^+$; calcd for $C_{20}H_{15}F_6N_3O_6S$: 539.4055; found 539.0605.

*4.4.7. N-[2-(2,6-Dichlorophenyl)-4-oxo-1,3-thiazolidin-3-yl]-2,5-bis(2,2,2-trifluoroethoxy)benzamide (**5g**).* White microcrystals; mp 116−117 °C; IR (KBr) γ/cm^{-1}: 3404 (NH), 3051 (ArC−H), 2986 (C−H), 1680 (C═O of thiazolidine), 1718 (C═O NH), 1266 (C−O−C); ^{1}H NMR ($CDCl_3$, 400 MHz): δ 9.08 (s, 1H,NH), 7.73 (d, 1H, Parent Ar−H), 7.12−7.19 (m, 2H, substituted Ar−H), 7.00−7.09 (m, 1H, substituted Ar−H), 6.87 (d, *J* = 9.0 Hz, 1H, Parent Ar−H), 6.72 (s, 1H, Parent Ar−H), 4.33−4.48 (m, 4H, CH_2CF_3), 3.75−3.89 (m, 2H, CH_2 of thiazolidinone); ^{13}C NMR ($CDCl_3$, 100 MHz): δ 29.65 (CH_2 of thiazolidine), δ 59.31 (CH of thiazolidine), δ 66.17−67.25 (quartet, $^2J_{CF}$ = 36.4 Hz,CH_2CF_3), δ 120.95 (quartet, $^1J_{CF}$ = 270 Hz,CF_3-coupling), δ 122.95 (C_1 of side chain Ar), δ 125.88 (C_1 of Ar), δ 130.71−130.62 ($C_{2,6}$ of side chain Ar), δ 153.01,150.33 ($C_{2,5}$ of Ar), δ 163.18(C═O of thiazolidine), δ 168.74(NH−C═O); HRMS (ESI, *m*/*z*): 569.0158 $[M + Li-H]^+$; calcd for $C_{20}H_{14}Cl_2F_6N_2O_4S$: 563.2975; found 563.0827.

*4.4.8. N-[2-(4-Methoxyphenyl)-4-oxo-1,3-thiazolidin-3-yl]-2,5-bis(2,2,2-trifluoroethoxy)benzamide (**5h**).* White microcrystals; mp 106−108 °C; IR (KBr) γ/cm^{-1}: 3400(NH), 3099(ArC−H), 3005 (C−H), 1666 (C═O of thiazolidine ring), 1707 (C═O NH), 1285 (C−O−C); ^{1}H NMR ($CDCl_3$, 400 MHz): δ 8.88 (s, 1H, NH), 7.69 (d, 1H, Parent Ar−H), 7.35 (s, 4H, substituted Ar−H), 7.12 (dd, *J* = 9.0, 3.3 Hz, 1H, Parent Ar−H), 6.85 (d, *J* = 9.2 Hz, 1H, Parent Ar−H), 5.98 (s, *J* = 1.2 Hz, 1H, CH of thiazolidinone), 4.17−4.40 (m, 4H, CH_2CF_3), 3.80 (ddd, *J* = 50.6, 15.9, 1.2 Hz, 2H,CH_2 of thiazolidinone); ^{13}C NMR ($CDCl_3$, 100 MHz): δ 30.18 (CH_2 of thiazolidine), δ 30.92 (OCH_3),δ 55.32 (CH of thiazolidine), δ 62.69−67.50 (quartet, $^2J_{CF}$ = 36 Hz,CH_2CF_3), δ 114.40,115.67 ($C_{3,5}$ of side chain Ar), δ 117.09(quartet, $^1J_{CF}$ = 268 Hz,CF_3-coupling), δ 115.67 (C_4 of Ar), δ 121.22(C_3 of Ar), δ 122.13 (C_6 of Ar), δ 129.15 (C_1 of side chain Ar), δ 128.56 (C_1 of Ar), δ 160.56(C_4 of side chain Ar), δ 153.12,150.34 ($C_{2,5}$ of Ar), δ 162.66(C═O of thiazolidine), δ 169.57 (NH−C═O); HRMS (ESI, *m*/*z*): 525.0912 $[M + H]^+$; calcd for $C_{21}H_{18}F_6N_2O_5S$: 524.4334; found 524.842.

4.5. Molecular Docking Studies. Molecular docking can offer information about how the drug molecules and proteins interact. The crystal structures of AURKA and VEGFR-2 were retrieved from the RCSB Protein Data Bank. The 1,3-thiazolidine-4-one derivatives were docked to the binding sites of AURKA and VEGFR-2 proteins using AutoDock Vina.[38] AutoDock GUI[39] was used to prepare the protein coordinate by eliminating water and cocrystallized ligands. The three-dimensional (3D) structures of 1,3-thiazolidine-4-one derivatives were optimized by B3LYP level 37 and 6-31G(d,p) basis set[40] using the Gaussian 09 package. At the binding pocket of the proteins, a 3D grid with a spacing of 0.375 Å was produced using Auto Grid. For the binding locations for AURKA and VGEFR-2, the grid box dimensions were set to 70 Å × 64 Å × 64 Å and 60 Å × 64 Å × 60 Å, respectively. In the docking process, both proteins were regarded as rigid. The confirmation of the 1,3-thiazolidine-4-one derivatives with the lowest binding energy at the protein-binding site was considered to be a favorable drug candidate. Moreover, ADMET prediction was used for the synthesized compounds to determine the safety, effectiveness, and bioavailability of the therapeutic candidates using the SwissADME web tool.[41] Lipinski's rule of five was employed to assess the compound's drug-likeness.[42]

4.6. Protocol for Molecular Dynamics Simulation. Molecular dynamics simulation is a crucial tool for more precise prediction of protein−drug interactions.[43,44] Based on experimental findings and docking data, the most active (**5e**) and moderately active (**5h**) ligands from the chosen synthesized compounds were used to explore the protein−drug interactions. Dynamic simulation studies were executed for AURKA/5e and AURKA/5h protein complexes by GROMACS 2018.4 software[45] using the AMBER99SB-ILDN force field[46] and TIP3P water model.[47] A periodic cubic box was used to solvate the protein−ligand combination, with the protein's distance from the box boundary being 1 nm. To utilize as little energy as possible, the steepest descent technique was applied after Na^+ ions were used to neutralize the system charge. At a time step of 2 fs, a 10 ns equilibration of NVT (at 300 K) and NPT (at 300 K and 1 atm) was performed. The short-range van der Waals cutoff was established at 1.2 nm, and the long-range electrostatic interactions were determined using the particle mesh Ewald technique.[48] The link containing hydrogen atoms was restrained using LINCS constraints.[49] The production run was then extended by 100 ns, until the protein RMSD converged. Further, using the same simulation protocol, the complexes of the most active (**5e**) and moderately active (**5h**) ligands were studied to understand the ligand binding at the VEGFR-2 binding site. Until convergence of the protein RMSD, a 60 ns production run was carried out for both complexes.

4.7. Cytotoxic Assay for Anticancer Studies. *4.7.1. Cell Culture.* Glioblastoma LN229 cells from humans were cultured in DMEM high-glucose media (HiMedia, cat. no. AL007S) supplemented with 10% heat-inactivated fetal bovine serum (FBS) (HiMedia, cat. no. RM10432), and 1% antibacterial and

https://doi.org/10.1021/acsomega.3c04662
ACS Omega 2023, 8, 43596−43609

Anti-Mycotic solution. Cells were kept at 37 °C with 5% CO_2, and growth media was replaced every 2 days. For cytotoxic experiments, the cells were subcultured once they had reached 70−80% confluence.

4.7.2. MTT Assay. A cell density of 0.03×10^6 cells/well of LN229 glioblastoma cells was used for the cytotoxicity assay. Cells are treated with these derivatives, consisting of 8 compounds, at varying concentrations of 5, 10, 15, 20, and 25 μM after the confluence of the cells has reached 70−80%. The cell viability of LN229 was assessed using the MTT test after 48 h of incubation at 37 °C in 5% CO_2. In brief, to each well, 0.5 mg/mL solution of MTT (3-(4,5-dimethylthiazol-2-yl)-2,5-diphenyltetrazolium bromide) was added. After 4 h of incubation, the MTT solution was withdrawn, and the purple crystal formazan forms were dissolved by adding 300 μL of a solubilizing buffer. At 570 nm, absorbance readings were determined after shaking the plates. Three concurrent experiments produced three findings, shown as mean ± standard deviation.[50−52]

4.7.3. IC_{50} Concentration Estimation for Newly Synthesized Compounds. After each treatment, the obtained absorbance values were employed in regression analysis of nonlinear type with the help of the GraphPad Prism software to estimate the IC50 values for each chemical (version 8.3.0). To do the nonlinear regression analysis, the MTT experiment's triplicate absorbance results were extracted into the *XY* sheet, where the values of *X* (concentration) were converted to logarithms and the values of *Y* (absorbance) were normalized.

4.7.4. Colony Formation Assay. The colony formation assay, also referred to as the clonogenic assay, is a test for in vitro cell survival that relies on the ability of a cell to form a colony. This experiment examined the capacity of cancer cells to sustain reproductive integrity over a prolonged length of time.[53] Trypsinized LN229 cells were plated at a consistent density of 50 cells per well on a 24-well plate. The change of medium was done to 5% FBS media, and then the studied compounds were added with minimum and maximum concentrations of 10 and 25 μM (depending on the findings of the MTT assay) and cultivated at 37 °C. The former colonies were stained with 0.5% crystal violet after 15 days of incubation, and the "Promega colony counter" web application tool was used to manually count the colonies.[54]

4.7.5. Tunnel Assay. Utilizing the tunnel test, the chosen samples from the MTT assay were assessed. With the use of this technique, particular endonucleases that cleave genomic DNA in the space between nucleosomes during apoptosis can be identified. Utilizing the Elabscience one-step TUNEL test kit, the selected molecules were examined for their capacity to cause cell apoptosis (catalog no: E-CK-A320).

4.7.6. Statistical Analysis. One-way analysis of variance (ANOVA) was used to evaluate all of the data, which were examined using GraphPad Prism 8.3.0. (nonparametric or mixed). Data from at least three separate experiments are given as the mean and standard deviation (error bars). $P < 0.05$.

■ ASSOCIATED CONTENT

Supporting Information

The Supporting Information is available free of charge at https://pubs.acs.org/doi/10.1021/acsomega.3c04662.

Estimated ADMET characteristics of the molecules and all spectral analysis such as IR, ^{1}H NMR, ^{13}C NMR, and HRMS (PDF)

■ AUTHOR INFORMATION

Corresponding Author

Arun M. Isloor − *Medicinal Chemistry Laboratory, Department of Chemistry, National Institute of Technology Karnataka, Mangalore 575 025, India;* orcid.org/0000-0003-2038-3494; Email: isloor@yahoo.com

Authors

Sathyanarayana D Shankara − *Medicinal Chemistry Laboratory, Department of Chemistry, National Institute of Technology Karnataka, Mangalore 575 025, India*

Pavan K. Jayaswamy − *Central Research Laboratory, K.S. Hegde Medical Academy, Nitte (Deemed to be University), Mangalore 575018 Karnataka, India*

Praveenkumar Shetty − *Central Research Laboratory, K.S. Hegde Medical Academy, Nitte (Deemed to be University), Mangalore 575018 Karnataka, India; Department of Biochemistry, K.S. Hegde Medical Academy, Nitte (Deemed to be University), Mangalore 575018 Karnataka, India*

Debashree Chakraborty − *Biophysical and Computational Chemistry Laboratory, Department of Chemistry, National Institute of Technology Karnataka, Mangalore 575025, India;* orcid.org/0000-0002-0142-7941

Pushyaraga P. Venugopal − *Biophysical and Computational Chemistry Laboratory, Department of Chemistry, National Institute of Technology Karnataka, Mangalore 575025, India*

Complete contact information is available at: https://pubs.acs.org/10.1021/acsomega.3c04662

Author Contributions

Material preparation, data collection, and analysis were performed by S.D.S. Supervision of the entire research project was performed by A.M.I. Anticancer studies were conducted by P.K.J. Supervision of anticancer studies was performed by P.S. Docking and simulation studies were done by P.P.V. Supervision of the docking and simulation studies was done by D.C. The final version of the manuscript was written by S.D.S. and A.M.I. All authors have read and agreed to the published version of the manuscript.

Notes

The authors declare no competing financial interest.

■ ACKNOWLEDGMENTS

The authors thank the Director of the National Institute of Technology Karnataka, Surathkal, India, for providing the research facilities. They also thank the "High-resolution Mass Spectrometer Facility-VIT, Vellore" for providing the HRMS facility.

■ REFERENCES

(1) Rai, U. S.; Isloor, A. M.; Shetty, P.; Pai, K.; Fun, H.-K. Synthesis and in vitro biological evaluation of new pyrazole chalcones and heterocyclic diamides as potential anticancer agents. *Arabian J. Chem.* **2015**, *8* (3), 317−321.

(2) Shankara, S. D.; Isloor, A. M.; Kudva, A. K.; Raghu, S. V.; Jayaswamy, P. K.; Venugopal, P. P.; Shetty, P.; Chakraborty, D. 2, 5-Bis (2, 2, 2-trifluoroethoxy) phenyl-tethered 1, 3, 4-Oxadiazoles Derivatives: Synthesis, In Silico Studies, and Biological Assessment as Potential Candidates for Anti-Cancer and Anti-Diabetic Agent. *Molecules* **2022**, *27* (24), No. 8694.

(3) Wilson, D. M., III; Deacon, A. M.; Duncton, M. A.; Pellicena, P.; Georgiadis, M. M.; Yeh, A. P.; Arvai, A. S.; Moiani, D.; Tainer, J. A.; Das, D. Fragment-and structure-based drug discovery for developing

therapeutic agents targeting the DNA Damage Response. *Prog. Biophys. Mol. Biol.* **2021**, *163*, 130−142.
(4) Sunil, D.; Isloor, A. M.; Shetty, P.; Satyamoorthy, K.; Prasad, A. B. 6-[3-(4-Fluorophenyl)-1H-pyrazol-4-yl]-3-[(2-naphthyloxy) methyl][1, 2, 4] triazolo [3, 4-b][1, 3, 4] thiadiazole as a potent antioxidant and an anticancer agent induces growth inhibition followed by apoptosis in HepG2 cells. *Arabian J. Chem.* **2010**, *3* (4), 211−217.
(5) Liu, Y.; Lu, Y.; Wang, J.; Xie, L.; Li, T.; He, Y.; Peng, Q.; Qin, X.; Li, S. Association between nonsteroidal anti-inflammatory drug use and brain tumor risk: a meta-analysis. *Br. J. Clin. Pharmacol.* **2014**, *78* (1), 58−68.
(6) Newlands, E. S.; Stevens, M. F. G.; Wedge, S. R.; Wheelhouse, R. T.; Brock, C. Temozolomide: a review of its discovery, chemical properties, pre-clinical development and clinical trials. *Cancer Treat. Rev.* **1997**, *23* (1), 35−61.
(7) Sathornsumetee, S.; Rich, J. N. Designer therapies for glioblastoma multiforme. *Ann. N. Y. Acad. Sci.* **2008**, *1142* (1), 108−132.
(8) Stupp, R.; Mason, W. P.; Van Den Bent, M. J.; Weller, M.; Fisher, B.; Taphoorn, M. J.; Belanger, K.; Brandes, A. A.; Marosi, C.; Bogdahn, U.; et al. Radiotherapy plus concomitant and adjuvant Temozolomide for glioblastoma. *N. Engl. J. Med.* **2005**, *352* (10), 987−996.
(9) da Silva, D. S.; da Silva, C. E. H.; Soares, M. S. P.; Azambuja, J. H.; de Carvalho, T. R.; Zimmer, G. C.; Frizzo, C. P.; Braganhol, E.; Spanevello, R. M.; Cunico, W. Thiazolidin-4-ones from 4-(methylthio)benzaldehyde and 4-(methylsulfonyl)benzaldehyde: Synthesis, antiglioma activity and cytotoxicity. *Eur. J. Med. Chem.* **2016**, *124*, 574−582.
(10) Sawyers, C. Targeted cancer therapy. *Nature* **2004**, *432* (7015), 294−297.
(11) Dominguez-Brauer, C.; Thu, K. L.; Mason, J. M.; Blaser, H.; Bray, M. R.; Mak, T. W. Targeting mitosis in cancer: emerging strategies. *Mol. Cell* **2015**, *60* (4), 524−536.
(12) Vader, G.; Lens, S. M. A. The Aurora kinase family in cell division and cancer. *Biochim. Biophys. Acta, Rev. Cancer* **2008**, *1786* (1), 60−72.
(13) Dar, A. A.; Goff, L. W.; Majid, S.; Berlin, J.; El-Rifai, W. Aurora kinase inhibitors-rising stars in cancer therapeutics? *Mol. Cancer Ther.* **2010**, *9* (2), 268−278.
(14) Katayama, H.; Sen, S. Aurora kinase inhibitors as anticancer molecules. *Biochim. Biophys. Acta, Gene Regul. Mech.* **2010**, *1799* (10), 829−839.
(15) Pradhan, T.; Gupta, O.; Singh, G.; Monga, V. Aurora kinase inhibitors as potential anticancer agents: Recent advances. *Eur. J. Med. Chem.* **2021**, *221*, No. 113495.
(16) Xu, C.; Wu, X.; Zhu, J. VEGF promotes proliferation of human glioblastoma multiforme stem-like cells through VEGF receptor 2. *Sci. World J.* **2013**, *2013*, 1−8, DOI: 10.1155/2013/417413.
(17) Fontanella, C.; Ongaro, E.; Bolzonello, S.; Guardascione, M.; Fasola, G.; Aprile, G. Clinical advances in the development of novel VEGFR2 inhibitors. *Ann. Transl. Med.* **2014**, *2* (12), 123.
(18) Hamerlik, P.; Lathia, J. D.; Rasmussen, R.; Wu, Q.; Bartkova, J.; Lee, M.; Moudry, P.; Bartek, J., Jr; Fischer, W.; Lukas, J.; Rich, J. N.; Bartek, J. Autocrine VEGF−VEGFR2−Neuropilin-1 signaling promotes glioma stem-like cell viability and tumor growth. *J. Exp. Med.* **2012**, *209* (3), 507−520.
(19) Kessler, T.; Sahm, F.; Blaes, J.; Osswald, M.; Rübmann, P.; Milford, D.; Urban, S.; Jestaedt, L.; Heiland, S.; Bendszus, M.; et al. Glioma cell VEGFR-2 confers resistance to chemotherapeutic and antiangiogenic treatments in PTEN-deficient glioblastoma. *Oncotarget* **2015**, *6* (31), 31050−31068.
(20) Ayati, A.; Emami, S.; Asadipour, A.; Shafiee, A.; Foroumadi, A. Recent applications of 1, 3-thiazole core structure in the identification of new lead compounds and drug discovery. *Eur. J. Med. Chem.* **2015**, *97*, 699−718.
(21) Isloor, A. M.; Sunil, D.; Shetty, P.; Malladi, S.; Pai, K. S. R.; Maliyakkl, N. Synthesis, characterization, anticancer, and antioxidant activity of some new thiazolidin-4-ones in MCF-7 cells. *Med. Chem. Res.* **2013**, *22* (2), 758−767.
(22) Pyrih, A.; Jaskolski, M.; Gzella, A. K.; Lesyk, R. Synthesis, structure and evaluation of anticancer activity of 4-amino-1,3-thiazolinone/pyrazoline hybrids. *J. Mol. Struct.* **2021**, *1224*, No. 129059.
(23) Jassem, A. M.; Dhumad, A. M.; Salim, J. K.; Jabir, H. A. An alternative technique for cyclization synthesis, in vitro anti-esophageal cancer evaluation, and molecular docking of novel thiazolidin-4-one derivatives. *J. Mol. Struct.* **2023**, *1280*, No. 135079.
(24) Farghaly, T. A.; Abbas, E. M. H.; Al-Soliemy, A. M.; Sabour, R.; Shaaban, M. R. Novel sulfonyl thiazolyl-hydrazone derivatives as EGFR inhibitors: Design, synthesis, biological evaluation and molecular docking studies. *Bioorg. Chem.* **2022**, *121*, No. 105684.
(25) Asati, V.; Bharti, S. K. Design, synthesis and molecular modeling studies of novel thiazolidine-2,4-dione derivatives as potential anti-cancer agents. *J. Mol. Struct.* **2018**, *1154*, 406−417.
(26) Petrou, A.; Eleftheriou, P.; Geronikaki, A.; Akrivou, M. G.; Vizirianakis, I. Novel thiazolidin-4-ones as potential non-nucleoside inhibitors of HIV-1 reverse transcriptase. *Molecules* **2019**, *24* (21), No. 3821.
(27) Abdellatif, K. R. A.; Abdelgawad, M. A.; Elshemy, H. A. H.; Alsayed, S. S. R. Design, synthesis and biological screening of new 4-thiazolidinone derivatives with promising COX-2 selectivity, anti-inflammatory activity and gastric safety profile. *Bioorg. Chem.* **2016**, *64*, 1−12.
(28) Trotsko, N. Antitubercular properties of thiazolidin-4-ones−A review. *Eur. J. Med. Chem.* **2021**, *215*, No. 113266.
(29) Younis, M. H.; Mohammed, E. R.; Mohamed, A. R.; Abdel-Aziz, M. M.; Georgey, H. H.; Gawad, N. M. A. Design, synthesis and anti-Mycobacterium tuberculosis evaluation of new thiazolidin-4-one and thiazolo [3, 2-a][1, 3, 5] triazine derivatives. *Bioorg. Chem.* **2022**, *124*, No. 105807.
(30) Gummidi, L.; Kerru, N.; Ebenezer, O.; Awolade, P.; Sanni, O.; Islam, M. S.; Singh, P. Multicomponent reaction for the synthesis of new 1, 3, 4-thiadiazole-thiazolidine-4-one molecular hybrids as promising antidiabetic agents through α-glucosidase and α-amylase inhibition. *Bioorg. Chem.* **2021**, *115*, No. 105210.
(31) Liesen, A. P.; de Aquino, T. M.; Carvalho, C. S.; Lima, V. T.; de Araújo, J. M.; de Lima, J. G.; de Faria, A. R.; de Melo, E. J. T.; Alves, A. J.; Alves, E. W.; et al. Synthesis and evaluation of anti-Toxoplasma gondii and antimicrobial activities of thiosemicarbazides, 4-thiazolidinones and 1,3,4-thiadiazoles. *Eur. J. Med. Chem.* **2010**, *45* (9), 3685−3691.
(32) Pejović, A.; Minić, A.; Jovanović, J.; Pešić, M.; Komatina, D. I.; Damljanović, I.; Stevanović, D.; Mihailović, V.; Katanić, J.; Bogdanović, G. A. Synthesis, characterization, antioxidant and antimicrobial activity of novel 5-arylidene-2-ferrocenyl-1, 3-thiazolidin-4-ones. *J. Organomet. Chem.* **2018**, *869*, 1−10.
(33) Patial, B.; Chawla, A.; Sharma, R.; Akhter, R.; Sharma, P.; Kumar, R. A Review on Anti-Cancer Activity of Benzopyrazole and Thiazolidine-4-One Nucleus. *Int. J. Res. Appl. Sci. Biotechnol.* **2022**, *9* (3), 166−174.
(34) Sun, J.; Chen, Y.-H.; Liu, H.-Y.; Hondo, E.; Zhou, Y.; Wu, Y.-F. Thiazolidinedione: A privileged scaffold for the development of anticancer agents. *Curr. Top. Med. Chem.* **2021**, *21* (28), 2529−2545.
(35) Komatsu, Y.; Yoshino, T.; Yamazaki, K.; Yuki, S.; Machida, N.; Sasaki, T.; Hyodo, I.; Yachi, Y.; Onuma, H.; Ohtsu, A. Phase 1 study of efatutazone, a novel oral peroxisome proliferator-activated receptor gamma agonist, in combination with FOLFIRI as second-line therapy in patients with metastatic colorectal cancer. *Invest. New Drugs* **2014**, *32* (3), 473−480.
(36) Che, X.-H.; Chen, C.-L.; Ye, X.-L.; Weng, G.-B.; Guo, X.-Z.; Yu, W.-Y.; Tao, J.; Chen, Y.-C.; Chen, X. Dual inhibition of COX-2/5-LOX blocks colon cancer proliferation, migration and invasion in vitro. *Oncol. Rep.* **2016**, *35* (3), 1680−1688.
(37) Küçükgüzel, Ş. G.; Oruç, E. E.; Rollas, S.; Şahin, F.; Özbek, A. Synthesis, characterisation and biological activity of novel 4-

thiazolidinones, 1,3,4-oxadiazoles and some related compounds. *Eur. J. Med. Chem.* **2002**, *37* (3), 197−206.
(38) Trott, O.; Olson, A. J. AutoDock Vina: improving the speed and accuracy of docking with a new scoring function, efficient optimization, and multithreading. *J. Comput. Chem.* **2010**, *31* (2), 455−461.
(39) Morris, G. M.; Huey, R.; Lindstrom, W.; Sanner, M. F.; Belew, R. K.; Goodsell, D. S.; Olson, A. J. AutoDock4 and AutoDockTools4: Automated docking with selective receptor flexibility. *J. Comput. Chem.* **2009**, *30* (16), 2785−2791.
(40) Lee, C.; Yang, W.; Parr, R. G. Development of the Colle-Salvetti correlation-energy formula into a functional of the electron density. *Phys. Rev. B* **1988**, *37* (2), 785−789.
(41) Daina, A.; Michielin, O.; Zoete, V. SwissADME: a free web tool to evaluate pharmacokinetics, drug-likeness and medicinal chemistry friendliness of small molecules. *Sci. Rep.* **2017**, *7* (1), No. 42717.
(42) Lipinski, C. A. Lead-and drug-like compounds: the rule-of-five revolution. *Drug Discovery Today: Technol.* **2004**, *1* (4), 337−341.
(43) Das, B. K.; Chakraborty, D. Deciphering the competitive inhibition of dihydropteroate synthase by 8 marcaptoguanine analogs: enhanced potency in phenylsulfonyl fragments. *J. Biomol. Struct. Dyn.* **2021**, *40*, 13083−13102.
(44) Venugopal, P. P.; Chakraborty, D. Molecular mechanism of inhibition of COVID-19 main protease by β-adrenoceptor agonists and adenosine deaminase inhibitors using in silico methods. *J. Biomol. Struct. Dyn.* **2022**, *40* (11), 5112−5127.
(45) Abraham, M. J.; Murtola, T.; Schulz, R.; Páll, S.; Smith, J. C.; Hess, B.; Lindahl, E. GROMACS: High performance molecular simulations through multi-level parallelism from laptops to supercomputers. *SoftwareX* **2015**, *1*−*2*, 19−25.
(46) Lindorff-Larsen, K.; Piana, S.; Palmo, K.; Maragakis, P.; Klepeis, J. L.; Dror, R. O.; Shaw, D. E. Improved side-chain torsion potentials for the Amber ff99SB protein force field. *Proteins: Struct., Funct., Bioinf.* **2010**, *78* (8), 1950−1958.
(47) Mark, P.; Nilsson, L. Structure and dynamics of the TIP3P, SPC, and SPC/E water models at 298 K. *J. Phys. Chem. A* **2001**, *105* (43), 9954−9960.
(48) Essmann, U.; Perera, L.; Berkowitz, M. L.; Darden, T.; Lee, H.; Pedersen, L. G. A smooth particle mesh Ewald method. *J. Chem. Phys.* **1995**, *103* (19), 8577−8593.
(49) Hess, B.; Bekker, H.; Berendsen, H. J.; Fraaije, J. G. LINCS: a linear constraint solver for molecular simulations. *J. Comput. Chem.* **1997**, *18* (12), 1463−1472.
(50) Meerloo, J. V.; Kaspers, G. J.; Cloos, J. Cell Sensitivity Assays: the MTT Assay. In *Cancer Cell Culture*; Springer, 2011; pp 237−245.
(51) Van Tonder, A.; Joubert, A. M.; Cromarty, A. D. Limitations of the 3-(4, 5-dimethylthiazol-2-yl)-2, 5-diphenyl-2H-tetrazolium bromide (MTT) assay when compared to three commonly used cell enumeration assays. *BMC Res. Notes* **2015**, *8* (1), No. 47.
(52) Sargent, J. M. The Use of the MTT Assay to Study Drug Resistance in Fresh Tumour Samples. In *Chemosensitivity Testing in Oncology*; Springer, 2003; Vol. *161*, pp 13−25.
(53) Rajendran, V.; Jain, M. V. In Vitro Tumorigenic Assay: Colony Forming Assay for Cancer Stem Cells. In *Cancer Stem Cells*; Springer, 2018; pp 89−95.
(54) Ikeda, M.; Longnecker, R. Pre-B-Cell Colony Formation Assay. In *DNA Viruses*; Springer, 2005; pp 279−283.

https://doi.org/10.1021/acsomega.3c04662
ACS Omega 2023, 8, 43596−43609